Dynamics of drying colloidal suspensions, measured by optical coherence tomography

Electronic Supplementary Information

Kohei Abe [a,d], Patrick Saul Atkinson [b], Chi Shing Cheung [b], Haida Liang [b], Lucas Goehring [b,*] and Susumu Inasawa [a,c,‡]

[a] Graduate School of Bio-Application and Systems Engineering, Tokyo University of Agriculture and Technology, 2-24-16 Naka-Cho, Koganei, Tokyo, 184-8588, Japan.

[b] School of Science and Technology, Nottingham Trent University, Clifton Lane, Nottingham, NG11 8NS, UK

[c] Department of Applied Physics and Chemical Engineering, Tokyo University of Agriculture and Technology

[d] Micro/Bio/Nanofluidics Unit, Okinawa Institute of Science and Technology Graduate University, 1919-1 Tan-cha, Onna, Kunigami, Okinawa, 904-0497, Japan.

Corresponding authors: * lucas.goehring@ntu.ac.uk (L. Goehring) and ‡ inasawa@cc.tuat.ac.jp (S. Inasawa)

S1. Prediction of particle concentration distribution from the collective diffusion coefficient

To predict the shape of the steady-state drying front for KE-W10 from Eq. (2), the gradient of the particle concentration distribution at φ was first taken as:

$$\frac{\mathrm{d}\varphi}{\mathrm{d}x} = \frac{(v-w)(\varphi-\varphi_0)}{D(\varphi)}. \qquad \text{(S1)}$$

Mass conservation also gives the following constraint,

$$v - w = -\frac{\varphi_\mathrm{f}}{\varphi_0}w, \qquad \text{(S2)}$$

where $\varphi_\mathrm{f} = 0.59$ is the filling factor of particles in the packed region. The film growth rate, w, corresponds to the slope of the plots in Fig. 5(a), which is 0.54 μm s^{-1}. Eq. (S2) and the fitted equation in Fig. 6(a) can be substituted into Eq. (S1). As a result, the following equation can be derived:

$$\frac{\mathrm{d}\varphi}{\mathrm{d}x} = \frac{(-\varphi_\mathrm{f}w/\varphi_0)(\varphi-\varphi_0)}{3070\varphi^{2.80}D_0}, \qquad \text{(S3)}$$

where D_0 is Stokes-Einstein coefficient. We perform a numerical integration by taking $\mathrm{d}x \sim \Delta x$ to be a small but finite distance, in which case φ at the updated location $x + \Delta x$ can be written as:

$$\varphi(x+\Delta x) = \varphi(x) + \frac{(-\varphi_\mathrm{f}w/\varphi_0)(\varphi-\varphi_0)}{3070\varphi(x)^{2.80}D_0}\Delta x \qquad \text{(S4)}$$

Finally, we approximate the far-field boundary condition $\varphi \to \varphi_0 = 0.18$ by an initial value of $\varphi(x_0) = 0.18001$. Then $\varphi(x)$ is calculated from this point by applying Eq. (S4) in Δx =10 μm steps, and the resultant values of $\varphi(x)$ are shown as the solid line in the inset of Fig. 6(a).

Similar steps were followed to generate the predicted particle concentrations shown in Fig. S6, for SM-30.

S2. Movie captions

Movie S1

Drying of SM-30 suspension with the initial particle concentration (φ_0) of 0.06. Cell width W in the drying cell is 5 mm. 0.1 s in the movie corresponds to 2 min in real time.

Movie S2

Drying of SM-30 suspension at φ_0 = 0.19. Cell width W in the drying cell is 5 mm. 0.1 s in the movie corresponds to 2 min in real time.

Movie S3

Flow of SM-30 suspension at φ_0 = 0.06 with fluorescence tracer particles. The movie was taken at the packing front. 0.1 s in the movie corresponds to 5 s in real time.

Movie S4

Flow of SM-30 suspension at φ_0 = 0.19 with fluorescence tracer particles. The movie was taken at the packing front. 0.1 s in the movie corresponds to 5 s in real time.

S3. Supplemental figures

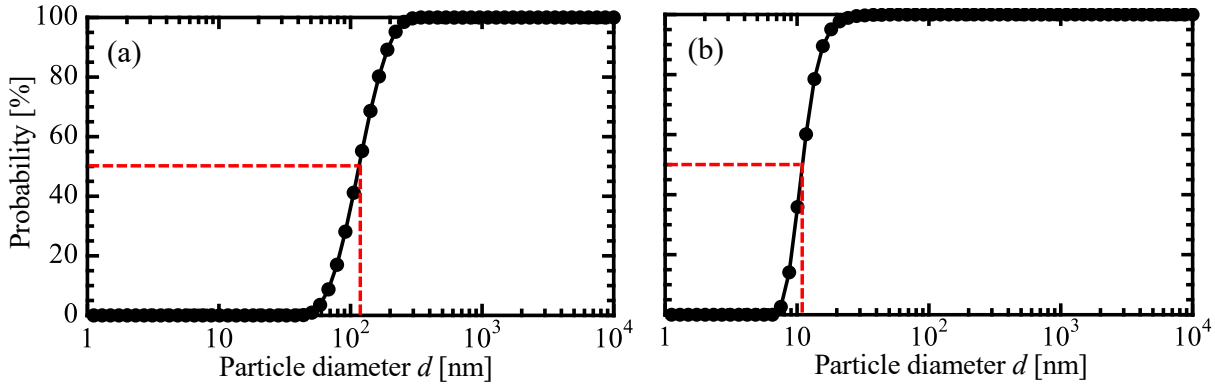

Fig. S1 Cumulative particle size distributions of (a) KE-W10 and (b) SM-30, as measured by dynamic light scattering. The mean particle sizes are indicated by red dashed lines.

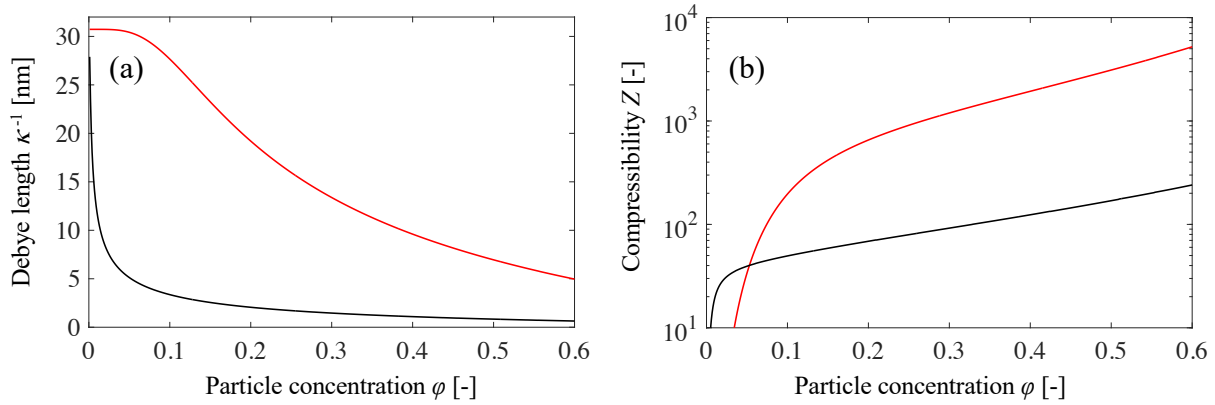

Fig. S2 (a) The effective Debye length κ^{-1} and (b) osmotic compressibility Z of the KEW-10 (red) and SM-30 (black) suspensions were modelled using the non-linear Poisson-Boltzmann cell model of Trizac et al. (2003), as implemented in Goehring, Li and Kiatkirakajorn (2017). The particles were assumed to have a bare (non-renormalized) surface charge density of 0.5 e^{-}/nm^2 and to be in Donnan equilibrium with a solution of monovalent salt of concentration 0.1 mM.

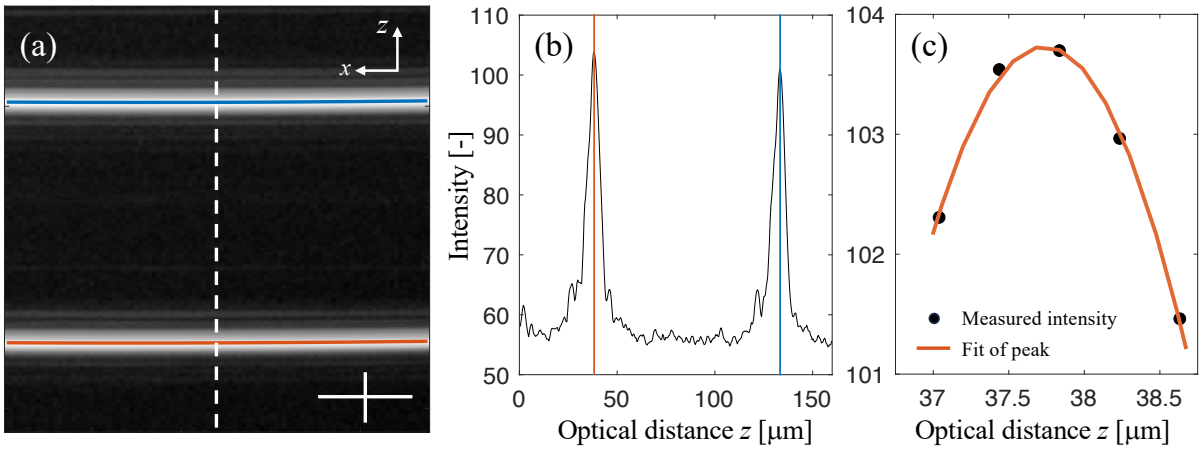

Fig. S3 Feature extraction. (a) An example region of interest from an OCT image of an empty cell, with scale bars showing 100 µm horizontally and 20 µm vertically. The depth profile (A-scan) along the dashed line is extracted and shown in panel (b), with the positions of the lower and upper interfaces of the Hele-Shaw cell given by orange and blue lines, respectively. At the lower interface, panel (c) shows the local intensity profile around the peak along with a Gaussian fit, which achieves sub-pixel accuracy.

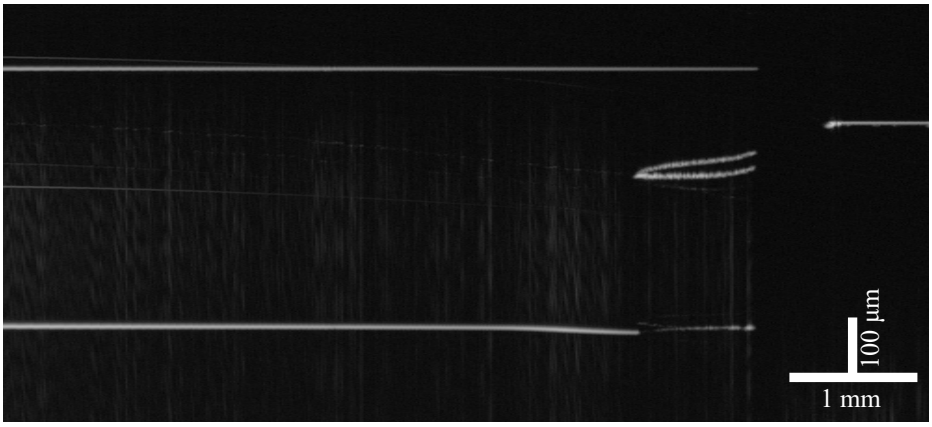

Fig. S4 A cross-sectional OCT image of drying SM-30 suspension (d = 10 nm) inside a drying cell where cell height H = 300 µm. The initial volume fraction of the suspension φ is 0.20 and the image was captured 40 min after the suspension is injected into the cell. An internal crack is visible on the upper-right of the image, appearing as two bright lines in proximity. The reflection from the suspension-glass interface below the crack is blurred and suppressed in intensity.

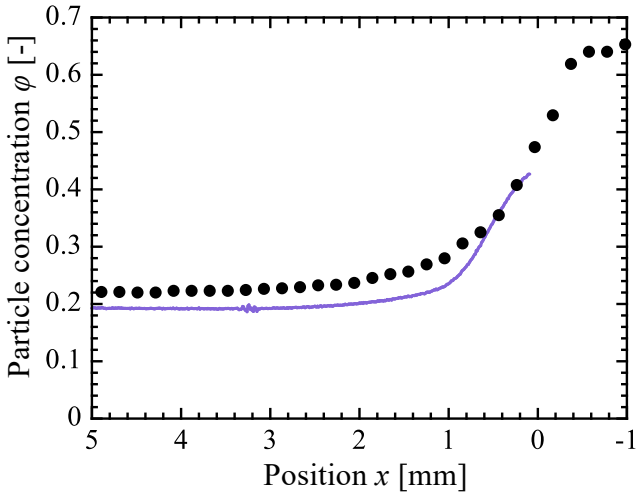

Fig. S5 Comparison of particle concentration measurements acquired with OCT (purple line, from Fig. 3(c) at t = 20 min) and data from a similar experiment observed with SAXS (black circles, data from Goehring, Li and Kiatkirakajorn (2017)). The data are aligned so that $\varphi = 0.42$ at $x = 0$. In both cases, Ludox SM-30 was measured in Hele-Shaw cells of thickness H = 300 μm, with evaporation rates estimated as 1.2 μm/s (OCT) 0.22 μm/s (SAXS). For the SAXS measurement the suspension had been dialysed against a 5 mM solution of NaCl. For OCT, no salt was added to the dialysis solution, apart from 0.1 mM NaOH to stabilize pH. Both data sets show consistent and comparable results, with the OCT giving better resolution (10 μm vs. 200 μm), but having difficulty with measurements once the film has solidified and cracked.

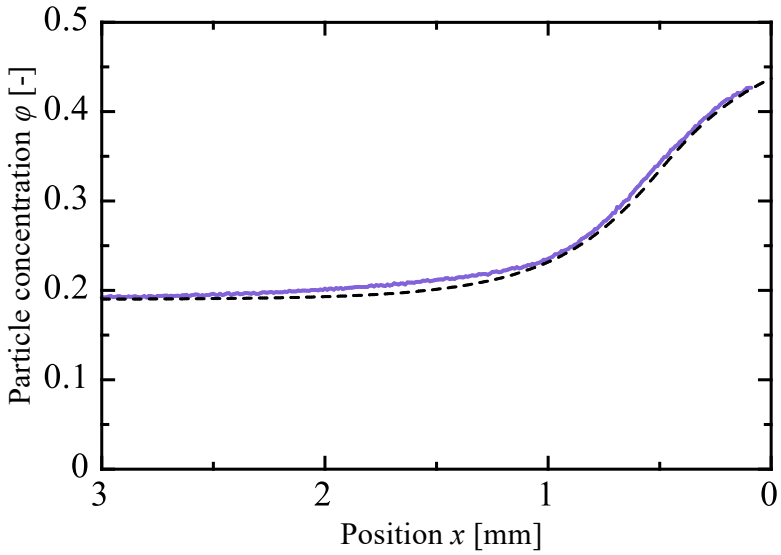

Fig. S6 The particle concentration distribution of SM-30 was estimated (dashed line) by integrating Eq. (2), using the fitting function given in Fig. 6(b) as $D(\varphi)$. The experimental result, acquired with OCT, is shown for comparison: purple solid line, at t = 40 min, data from Fig. 3(c).